Hyperbolic heat conduction, effective temperature, and third law for nonequilibrium systems with heat flux

S. L. Sobolev*

Institute of Problems of Chemical Physics, Academy of Sciences of Russia, Chernogolovka, Moscow Region, 142432 Russia

(Received 23 September 2017; published 15 February 2018)

Some analogies between different nonequilibrium heat conduction models, particularly random walk, the discrete variable model, and the Boltzmann transport equation with the single relaxation time approximation, have been discussed. We show that, under an assumption of a finite value of the heat carrier velocity, these models lead to the hyperbolic heat conduction equation and the modified Fourier law with relaxation term. Corresponding effective temperature and entropy have been introduced and analyzed. It has been demonstrated that the effective temperature, defined as a geometric mean of the kinetic temperatures of the heat carriers moving in opposite directions, acts as a criterion for thermalization and is a nonlinear function of the kinetic temperature and heat flux. It is shown that, under highly nonequilibrium conditions when the heat flux tends to its maximum possible value, the effective temperature, heat capacity, and local entropy go to zero even at a nonzero equilibrium temperature. This provides a possible generalization of the third law to nonequilibrium situations. Analogies and differences between the proposed effective temperature and some other definitions of a temperature in nonequilibrium state, particularly for active systems, disordered semiconductors under electric field, and adiabatic gas flow, have been shown and discussed. Illustrative examples of the behavior of the effective temperature and entropy during nonequilibrium heat conduction in a monatomic gas and a strong shockwave have been analyzed.

DOI: 10.1103/PhysRevE.97.022122

I. INTRODUCTION

Understanding how heat is carried, distributed, stored, and converted in various systems has occupied the minds of many scholars for quite a long time [1–14]. This is not due only to purely academic reasons: its practical importance in the fabrication and characterization of nanoscale systems has been recognized as one of the most critical programs in process industries [15–26]. The presence of the heat flux implies that the system is far from equilibrium. Building a general framework describing the far-from-equilibrium systems has led to a considerable amount of work towards this aim (Refs. [1–47] and references therein). In spite of recent advances, our current understanding of the fundamentals of nonequilibrium heat conduction still remains incomplete, and a complete understanding is undoubtedly far beyond what we know for equilibrium systems. Strictly speaking, a local temperature has a well-established meaning only in global equilibrium when the heat flux is zero. In particular, the question of what precisely is a "local temperature" in a nonequilibrium system, a concept that has a well-established meaning only in global equilibrium, is open to discussion [5,6,9,14–18,21–24,28–33,40–49]. Classical irreversible thermodynamics (CIT) is based on the local equilibrium assumption, which uses a local temperature defined as in global equilibrium even for the nonequilibrium situation with nonzero heat flux. The local equilibrium assumption is valid only for a relatively weak deviation from local equilibrium when the characteristic time scale of the process t significantly exceeds the relaxation time to local equilibrium τ, i.e., $t \gg \tau$. CIT leads to the well-known Fourier law (FL) for the heat flux and parabolic heat conduction equation (PHCE) for the local equilibrium temperature. However, there are two main motivations to go beyond the local equilibrium assumption. One of them, of a theoretical nature, refers to the so-called paradox of propagation of thermal signals with infinite speed, which is predicted by the PHCE [1,2,4,5,6]. The second, more closely related to experimental observations, deals with the propagation of second sound, ballistic phonon propagation, and phonon hydrodynamics in solids at low temperatures, where heat transport departs dramatically from the usual parabolic description [5–7,9–11,14–26]. The most simple and well-known modification of the Fourier law (MFL) for the one-dimensional (1D) case is given by [1,2,5–15]

$$q + \tau \frac{\partial q}{\partial t} = -\lambda \frac{\partial T}{\partial x} \tag{1}$$

where q is the heat flux, T is the temperature, and λ is the thermal conductivity. Equation (1) introduces a relaxation of the heat flux q with the characteristic time τ. The MFL, Eq. (1), together with the energy conservation law gives the hyperbolic heat conduction equation (HHCE) [1,2,5–15]:

$$\frac{\partial T}{\partial t} + \tau \frac{\partial^2 T}{\partial t^2} = a \frac{\partial^2 T}{\partial x^2} \tag{2}$$

where $a = \lambda/c$ is the thermal diffusivity, and c is the specific heat. As a consequence of the introduction of the term $\tau \partial q/\partial t$ in Eq. (1) or the corresponding term $\tau \partial^2 T/\partial t^2$ in Eq. (2), one obtains a finite velocity of propagation $v = \sqrt{a/\tau}$. The hyperbolic nature of the transfer equation (2) plays the most

*sobolev@icp.ac.ru

significant role at short times $t \sim \tau$. From the physical point of view, this corresponds to an initial condition where all particles move mutually in the same direction. After the characteristic time τ, the effect of the randomization of the particle motion becomes and Eq. (2) reduces to the standard PHCE, whereas Eq. (1) reduces to the FL.

Although Eqs. (1) and (2) overcome the paradox of an infinite velocity of heat propagation and have been used to describe heat transport in out-of-equilibrium systems for quite a long time, they still raise an important question: how is the local nonequilibrium temperature T defined? Can classical thermodynamic temperature, being a global equilibrium concept, still be invoked in the nonequilibrium process described by Eqs. (1) and (2)? The question "what is temperature?" has become a subject of intense theoretical and experimental interest in a more broad context of physics, chemistry, and life sciences [5,6,16–18,20–24,27–33,37–47,49]. Several effective nonequilibrium temperatures may be defined, all of which reduce to a common value in equilibrium states, but which yield different results in nonequilibrium situations. For example, in molecular dynamic (MD) simulations, which are often used to study heat flow under far-from-equilibrium conditions, the most important conceptual problem is how to define the temperature at different planes in the simulation cells. Usually the MD simulations define the temperature T on the basis of an average kinetic energy as [3,5,6,16–18,37–39]

$$\frac{3}{2}k_B T_i = \left\langle \frac{m v_i^2}{2} \right\rangle \tag{3}$$

where m is the mass of an atom, and v_i is the velocity of an atom at site i. The temperature defined on the basis of the kinetic energy of the particles is sometimes referred to as the kinetic temperature. The continuous approaches [28,42] also use an analogous definition of local nonequilibrium temperature based on the internal energy—the temperature of the local nonequilibrium state is the temperature of the equilibrium state with the same energy density as in the nonequilibrium state. These approaches assume that the energy density is related to temperature by $e = \int_0^T c d\xi$, where c is the heat capacity, and the temperature increase is calculated by $\Delta T = \Delta e/c$ provided that ΔT is moderate so that there is no phase change and the specific heat can be regarded as a constant [42]. In a more general case the relation between phonon energy and lattice temperature is obtained by the Debye model [16,27,38]. For glassy systems, the definition of the equilibrium temperature has been extended to the nonequilibrium regime, showing up as an effective quantity in a modified version of the fluctuation-dissipation theorem (FDT) [3,6,17,40]. Glasses are out-of-equilibrium systems in which thermal equilibrium is reached by work exchanged through thermal fluctuations and viscous dissipation exchange that happens at widely different time scales simultaneously. The "active" systems, from phase transformations [12,19,25] to biosystems [31,32,40,47], move actively by consuming energy from internal or external energy sources and their behavior is thus intrinsically out of equilibrium. The effective temperature of the active systems is usually defined on the basis of the FDT. Extended irreversible thermodynamics (EIT) [5,6,9,21] goes beyond the local equilibrium assumption and obtains generalized heat conduction models by introducing additional state variables, such as heat flux, into the expression of entropy. As a result the nonequilibrium temperature is introduced as $\theta_{\rm EIT} = (\partial S/\partial e)^{-1}$, where S is the local nonequilibrium entropy and e is the local energy density. The thermomass model (TMM) [41] indicates that the thermal energy is equivalent to a small amount of mass, called thermomass, according to Einstein's mass-energy equivalence relation and modifies the definition of entropy and temperature for nonequilibrium situations. The TMM [41] corresponds in many aspects to fluid hydrodynamics [4] and EIT [5,6,9,21].

In this paper we consider a 1D heat conduction when the deviation from local equilibrium is caused by the presence of heat flux. In Sec. II we briefly review and discuss some theoretical approaches, which take into account a finite value of the heat-mass carrier velocity, as an attempt to deepen the understanding of heat conduction under far-from-equilibrium conditions. In Sec. III the effective temperature and entropy for the far-from-equilibrium state are introduced and analyzed. Comparisons among different definitions of an effective temperature are carried out. In Sec. IV we use the results of Sec. III to illustrate the behavior of the effective temperature in some nonequilibrium situations. Concluding remarks are given in Sec. V.

II. MODELING

A. Random walk approach

The ordinary random walk (RW) or Brownian motion is completely characterized by the diffusion coefficient $D \propto h^2/\tau$, where h is the mean free path of the heat (mass) carriers and τ is the relaxation time. In the limit $h \to 0$ and $\tau \to 0$, the value of the diffusion coefficient is kept nonzero, which, in accordance with the parabolic type of the classical diffusion equation, implies an infinite velocity of diffusion particles $v = h/\tau \to \infty$. For local equilibrium processes with $t \gg \tau$ this physically unpleasant property does not play an important role. However, for relatively fast processes with $t \sim \tau$, a finite value of the particle velocity, which is a more reasonable concept from a physical point of view, should be taken into account. In one dimension a well-defined finite velocity of the diffusion particles v means that the system consists of two groups of particles—one group moves on the left and another moves on the right. This two group (TG) approach yields the evolution equations for the particle density as follows [1,2,12]:

$$\frac{\partial u_1}{\partial t} + v\frac{\partial u_1}{\partial x} = \frac{u_2 - u_1}{\tau}, \tag{4}$$

$$\frac{\partial u_2}{\partial t} - v\frac{\partial u_2}{\partial x} = \frac{u_1 - u_2}{\tau} \tag{5}$$

where $u_1(x,t)$ is the density of particles going to the right, $u_2(x,t)$ is the density of particles going to the left, v is the velocity of particles, and τ is the mean free time. For the following considerations it is convenient to rearrange Eqs. (4) and (5) as follows:

$$\frac{\partial u_1}{\partial t} + v\frac{\partial u_1}{\partial x} = -\frac{u_1 - u_0}{\tau_0}, \tag{6}$$

$$\frac{\partial u_2}{\partial t} - v\frac{\partial u_2}{\partial x} = -\frac{u_2 - u_0}{\tau_0} \tag{7}$$

where $u_0 = u/2$ with $u = u_1 + u_2$ being the total density of the particles, $\tau_0 = \tau/2$. After some algebra Eqs. (4) and (5) give

$$\frac{\partial u}{\partial t} + \frac{\partial J}{\partial x} = 0, \tag{8}$$

$$J + \frac{\tau}{2}\frac{\partial J}{\partial t} = -\frac{\tau}{2}v^2\frac{\partial u}{\partial x} \tag{9}$$

where J is the particle flux given by

$$J = v(u_1 - u_2). \tag{10}$$

Equation (10) allows us to represent u_1 and u_2 in terms of u and J as follows:

$$u_1 = (u + J/v)/2, \tag{11}$$

$$u_2 = (u - J/v)/2. \tag{12}$$

Introducing Eq. (9) into Eq. (8), which expresses conservation law in one dimension, we obtain

$$\frac{\partial u}{\partial t} + \frac{\tau}{2}\frac{\partial^2 u}{\partial t^2} = \frac{\tau}{2}v^2\frac{\partial^2 u}{\partial x^2}. \tag{13}$$

Taking into account that $\tau_0 = \tau/2$ and $D = v^2\tau/2 = v^2\tau_0$, with D being the diffusion coefficient, Eqs. (9) and (13) take the form analogous to Eqs. (1) and (2), respectively. Thus, the assumption of a finite value of the diffusing particle leads to the MFL and the HHCE [1,2,12,13,34].

B. Boltzmann transport equation

The Boltzmann transport equation (BTE) with the single relaxation time (or Bhatnagar-Gross-Krook) approximation is given by [6,10,18,24,37,38,42]

$$\frac{\partial f}{\partial t} + \vec{v}\cdot\vec{\nabla} f = -\frac{f - f^0}{\tau_0} \tag{14}$$

where f is the phonon distribution function, $\vec{v}$ is the phonon group velocity, and f^0 is the equilibrium distribution function. The BTE, Eq. (14), can be cast into an equation for the phonon energy density e by integrating it over the frequency spectrum as $e(T) = \sum_p \int f\hbar\omega_p D_p(\omega)d\omega$, where p is the polarization of phonons (acoustic and optical) and $D_p(\omega)$ is the phonon density of states per unit volume [37,38,42]. For simplicity, the effects of temperature on the dispersion relations and the phonon density of states are neglected. Then, the BTE in a phonon energy density (e) formulation for one dimension is given by [37,38,42]

$$\frac{\partial e}{\partial t} + v_x\frac{\partial e}{\partial x} = -\frac{e - e^0}{\tau_0} \tag{15}$$

where e^0 is the equilibrium phonon energy density, and v_x is the component of velocity along the x axis. Since in one dimension the phonons can travel in the positive or negative direction along the x axis, Eq. (15) gives two equations:

$$\frac{\partial e_1}{\partial t} + v\frac{\partial e_1}{\partial x} = -\frac{e_1 - e_1^0}{\tau_0}, \tag{16}$$

$$\frac{\partial e_2}{\partial t} - v\frac{\partial e_2}{\partial x} = -\frac{e_2 - e_2^0}{\tau_0}. \tag{17}$$

Taking into account that $e_i^0 = e/2$, it is evident that Eqs. (16) and (17) have analogous form as Eqs. (6) and (7), respectively. Moreover, after some algebra, as above, we obtain equations for the energy flux j and energy density e:

$$j + \tau_0\frac{\partial j}{\partial t} = -D\frac{\partial e}{\partial x}, \tag{18}$$

$$\frac{\partial e}{\partial t} + \tau_0\frac{\partial^2 e}{\partial t^2} = D\frac{\partial^2 e}{\partial x^2} \tag{19}$$

where the total phonon energy density is defined as the sum $e = e_1 + e_2$, while the energy flux is given as $j = v(e_1 - e_2)$.

Thus, the BTE with the single relaxation time approximation leads to the constitutive equation for the energy flux j, Eq. (18), and the evolution equation for the energy density e, Eq. (19), analogous to the MFL, Eq. (1), and the HHCE, Eq. (2).

Note that the transfer equation due to the BTE with the single relaxation time approximation, Eq. (19), is a partial differential equation of hyperbolic type. It contains both "relaxation" (or "wave") term $\tau\,\partial^2/\partial t^2$ and classical "diffusive" term $\partial^2/\partial x^2$, so the artificial inclusion of "an additional diffusive term" into the BTE model by Pisipati *et al.* [38] seems to be excessive.

C. Lattice Boltzmann method

Extensive computational effort is required to solve the BTE, since it involves seven independent variables descriptive for space, time, and momentum or velocity domain. This has led to the development of the lattice Boltzmann method (LBM) that, in essence, is a numerical scheme for solving the BTE, maintaining its accuracy while reducing the computational effort necessary to solve it [37,38,42]. One of the most popular schemes of LBM widely applied in classical phonon hydrodynamics is based on the BTE with the single relaxation time approximation, which, as it has been discussed above, results in the MFL and the HHCE for energy density (temperature). The HHCE describes the space-time evolution of the kinetic temperature under the local nonequilibrium conditions when the characteristic time of the process $t \sim \tau$, but the characteristic space scale of the process $L \gg h$. This corresponds to the work of Majumdar [24] that obtained the HHCE from semiclassical Boltzmann transport theory only in the acoustically thick limit when the characteristic space scale is much larger than the phonon mean free path. Since the LBM is a consequence of the BTE with the single relaxation time approximation and has the same accuracy, it is applicable, strictly speaking, to the local nonequilibrium case with $t \sim \tau$, but is not applicable to the space nonlocal situations when $L \sim h$. This implies that application of the LBM to heat conduction in nanofilms with $L \sim h$ needs additional justification.

D. Discrete variable model

Although the HHCE overcomes the dilemma of infinite thermal propagation speed of the classical parabolic heat-mass transfer equation, it, as we discussed above, cannot be applied to length scales comparable to the mean free path of energy carriers because of the breakdown of continuum approaches under severe nonequilibrium conditions. Therefore, it is desirable to adopt a method directly based on the microscopic view of

transport to deal with problems involving both small temporal and spatial scales. This method should also take into account another important issue of nanoscale heat conduction—the size of the region over which temperature is defined. The classical definition is entirely local, and one can define a temperature for each space point, whereas for the quantum definition the length scale is defined by the mean free path of the phonon [16]. The idea of the minimum space region to which the local temperature $T(x,t)$ can still be assigned corresponds to the conclusion of Majumdar [24] that "since temperature at a point can be defined only under local thermodynamic equilibrium, a meaningful temperature can be defined only at points separated on an average by the phonon mean free path." It is also consistent with the concept of a minimum heat affected region suggested by Chen [22], which assumes that during phonon transport from a nanoscale heat source the minimum size of the heat affected region is of the order of the phonon mean free path.

Cahill *et al.* [16] pointed out that in the nanoscale thermal transport the question "what is temperature?" is really a question about the size of the regions over which a local temperature can be defined. In molecular dynamics simulations of heat flow through grain boundaries the most important conceptual problem is how to define the temperature at different planes in the simulation cell. The MD simulations by different groups do show an abrupt change in the kinetic energy and, consequently, in the kinetic temperature of a plane of atoms at the twin boundary; regardless of which temperature scale is adopted, a graph of temperature versus distance shows an abrupt change [16]. Moreover, in agreement with Majumdar [24], Cahill *et al.* [16] also stated that for the quantum definition of temperature the length scale is defined by the mean free path h of the phonon and, consequently, a local region with a designated temperature must be larger than the phonon scattering distance. This phonon viewpoint of temperature implies that temperature cannot vary within a grain, or within a superlattice layer, on a scale smaller than h. If the layer thickness of the superlattice is less than h, then one cannot define $T(x)$ within this layer—the whole layer is probably at the same temperature [16].

The most simple approach to take into account the space and time nonlocality of the nonequilibrium thermal transport at micro- and nanoscales is the discrete variable model (DVM) [1,12,13,26,34–36,49], which discretizes the transport process in space and time by defining the minimum lattice size h to which the local temperature T can still be assigned and the minimum time τ (of the order of the mean free time of heat carriers) between the successive events of energy exchange. The DVM temperature cannot vary within a discrete layer on a scale h, i.e., one cannot define $T(x,t)$ within this layer because the whole layer is at the same temperature. This point is emphasized, since all theories of heat transport in superlattices have assumed that one could define a local temperature $T(x,t)$ within each layer [16,18]. One might argue that the DVM is analogous to the LBM because both models use discrete variables. However, as we discussed above, the LBM accuracy is of the order of the accuracy of the BTE with the single relaxation time approximation, which is local in space, whereas the DVM is inherently nonlocal and captures well the behavior of heat transport on short space ($L \sim h$) and time ($t \sim \tau$) scales [26].

The DVM gives the 1D energy transfer equation as follows [1,12,13,26,34–36]:

$$U(n+1,k) = \tfrac{1}{2}[U(n,k+1) + U(n,k-1)] \tag{20}$$

where $U(n,k)$ is the internal energy of a discrete layer k at a discrete time moment n. Continuum variables t and x are related with the corresponding discrete variables as follows: $t = n\tau$ and $x = kh$. Within a layer $k = x/h$, which in the continuum variables ranges from $(x - h/2)$ to $(x + h/2)$, the internal energy U and the corresponding temperature T do not change. In the continuum variables t and x, Eq. (20) is given by

$$U(t+\tau,x) = \tfrac{1}{2}[U(t,x+h) + U(t,x-h)]. \tag{21}$$

The discrete formalism implies that the energy exchange between the layers occurs on the border between the neighboring layers k and $k+1$ at an average time moment $(n+1/2)$, which gives the following equation for the energy flux j [12,13,26,34–36]:

$$j\left(n+\frac{1}{2},k,k+1\right) = \frac{v}{2}[U(n,k) - U(n,k+1)]. \tag{22}$$

Making for convenience a coordinate shift for continuum coordinate $x \to x + h/2$, we can present the heat flux q in terms of the continuum variables as follows:

$$j(t+\tau/2,x) = \frac{v}{2}[U(t,x-h/2) - U(t,x+h/2)] \tag{23}$$

where x is a coordinate of the border between the neighboring layers, the centers of which are at coordinates $x - h/2$ and $x + h/2$. Thus, the DVM is inherently nonlocal—it directly includes into the governing equations for the energy density, Eqs. (20) and (21), and for the heat flux, Eqs. (22) and (23), both time τ and space h scales of energy carriers.

Continuum limits

Equations (21) and (23) can be represented in an operator form as follows [13,26]:

$$[\exp(\tau\partial_t) - \cosh(h\partial_x)]e = 0, \tag{24}$$

$$\exp\left(\frac{\tau}{2}\partial_t\right)q = -\frac{v}{2}\sinh\left(\frac{h}{2}\partial_x\right)e \tag{25}$$

where e and q substitute for U and j, respectively, in the continuum representation. Taylor expansions of these equations in the continuum limit $h \to 0$ and $\tau \to 0$ contain an infinite number of terms with two small parameters h and τ. To obtain the corresponding equations with a finite number of terms one should first specify an invariant of the continuum limit, which conserves a desirable property of the continuum model.

a. Diffusive continuum limit $D = h^2/2\tau = const > 0$. In the continuum limit $h \to 0$ and $\tau \to 0$, Eq. (24) gives up to the first order in τ

$$\tau\frac{\partial e}{\partial t} = \tau D\frac{\partial^2 e}{\partial x^2} + o(\tau).$$

This equation corresponds to the classical heat conduction equation of parabolic type. The requirement that the heat diffusivity $h^2/2\tau$ has a finite value in the continuum limit

$h \to 0$ and $\tau \to 0$ implies that the velocity of the heat carriers $v = h/\tau \to \infty$. Indeed, representing v as $v = 2a/h$, we obtain that $v \to \infty$ at $h \to 0$ when a is nonzero. This is the so-called paradox of propagation of energy disturbances with infinite speed discussed above.

b. Wave continuum limit $v = h/\tau = const < \infty$. An alternative type of the continuum limit, which guarantees a finite value of the heat-carrier velocity v, requires that $v = h/\tau =$ const $< \infty$ at $h \to 0$ and $\tau \to 0$ [12,13,34–36]. In this case Eq. (24) gives up to the first order in τ

$$\frac{\partial e}{\partial t} + \frac{\tau}{2}\frac{\partial^2 e}{\partial t^2} = \frac{\tau}{2}v^2\frac{\partial^2 e}{\partial x^2} + o(\tau). \tag{26}$$

Equation (26) is of hyperbolic type and is analogous to Eq. (13) obtained from the RW approach and to Eq. (19) obtained from the BTE with the single relaxation time approximation. The corresponding continuum limit of Eq. (25) gives

$$j + \frac{\tau}{2}\frac{\partial q}{\partial t} = -\frac{\tau}{2}v^2\frac{\partial e}{\partial x} + o(\tau) \tag{27}$$

which also corresponds to the result of the RW, Eq. (9), and the BTE with the single relaxation time approximation, Eq. (18).

c. Temperature representation. Assuming the constant specific heat c and using the kinetic definition of the temperature $T \propto e/c$, one obtains that Eqs. (27) and (28) reduce exactly to the HHCE, Eq. (2), and the MFL, Eq. (1), respectively. In terms of the TG picture discussed in the previous sections, the DVM provides the following expressions for the heat flux q [see Eq. (23)] and the kinetic temperature T [see Eq. (21)]:

$$q = vc(T_1 - T_2)/2, \tag{28}$$

$$T = (T_1 + T_2)/2 \tag{29}$$

where T_1 and T_2 are the kinetic temperatures of the two groups of the heat carriers moving in opposite directions. Equations (28) and (29) can be presented in a slightly different form as

$$T_1 = T + q/vc, \tag{30}$$

$$T_2 = T - q/vc. \tag{31}$$

Kroneberg *et al.* [28] also assume the TG model and arrive at Eqs. (30) and (31), as well as at the HHCE, Eq. (2), using the energy equations for T_1 and T_2 analogous to Eqs. (4) and (5). Thus, the DVM with the "wave" law of the continuum limit leads to the HHCE, Eq. (2), and the MFL, Eq. (1).

To conclude this section, it should be noted that the RW [1,2,12,13], the TG representation of Kroneberg *et al.* [28], the BTE with the single relaxation time approximation [28,37,38,42], and the DVM at the wave law of the continuum limit [12,13,34–36] lead to the HHCE, Eq. (2), and the MFL, Eq. (1), due to the assumption of the finite value of the heat carrier velocity.

III. RESULTS AND DISCUSSION

A. Effective temperature θ

The kinetic temperature T, the space-time evolution of which is governed by the HHCE, Eq. (2), characterizes the local energy density of the nonequilibrium state—it is equal to the equilibrium temperature of the same system with the same internal energy in equilibrium. In terms of the TG approach it implies that if a local volume element of the nonequilibrium system consisting of the two groups of the heat carriers with the temperatures T_1 and T_2 is suddenly isolated, i.e., bounded by adiabatic and rigid walls, and allowed to relax to equilibrium, after equilibration the equilibrium temperature of the local element will be $T_{\rm eq} = (T_1 + T_2)/2$. However, if the two groups of the heat carriers with T_1 and T_2 equilibrate reversibly, i.e., while producing work, their common equilibrium temperature $\bar{T}_{\rm eq}$ will be [3,9,33]

$$\bar{T}_{\rm eq} = (T_1 T_2)^{1/2}. \tag{32}$$

Indeed, before equilibration the total equilibrium entropy of the two groups is equal to $S_{\rm eq} = k_B \ln T_1 + k_B \ln T_2 = k_B \ln T_1 T_2$, whereas after equilibration $\bar{S}_{\rm eq} = 2k_B \ln \bar{T}_{\rm eq}$. The entropy change during the equilibration is $\Delta S = S_{\rm neq} - S_{\rm eq} = k_B \ln T_1 T_2/\bar{T}_{\rm eq}^2$. When the system equilibrates reversibly, the entropy does not change, i.e., $\Delta S = 0$, and the last expression gives Eq. (32) [33,49].

Multiplying Eq. (30) by Eq. (31), we obtain the following nonlinear expression for the effective temperature θ of the nonequilibrium state as [9]

$$\theta^2 = T^2 - (q/cv)^2. \tag{33}$$

Introducing the nondimensional heat flux $\hat{q}$ as $\hat{q} = q/vcT$, one can represent Eq. (33) in the form

$$\theta/T = (1 - \hat{q}^2)^{1/2}. \tag{34}$$

Note that $\hat{q} = 1$ corresponds to the maximum possible value of the heat flux $q^{\max} = vcT$, which is reached when all the heat carriers move in the same direction [6,8,27]. Figure 1 shows the nondimensional effective temperature θ/T as a function of the nondimensional heat flux $\hat{q}$ (solid line). In equilibrium $\hat{q} = 0$ and, as expected, Eq. (34) gives $\theta = T$. When the heat flux increases, the effective temperature θ/T decreases. When $\hat{q} \to 1$, Eq. (34) predicts $\theta \to 0$ (see solid line in Fig. 1), which implies that the real positive values of the effective temperature θ correspond to a physically reasonable upper bound on the heat flux $|q| \leqslant q^{\max}$. The limit also gives $T_1 \to 2T$ and $T_2 \to 0$ [see Eqs. (30) and (31)].

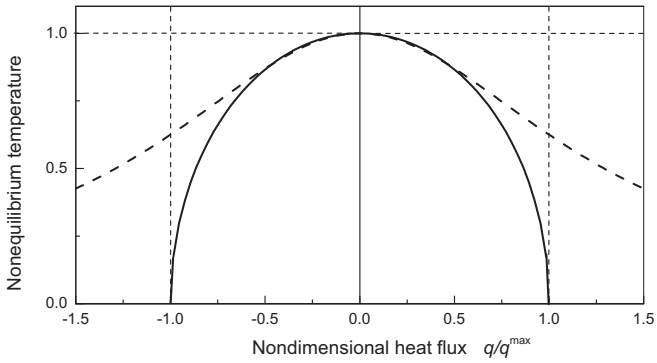

FIG. 1. Nondimensional effective temperature θ/T as a function of the nondimensional heat flux $\hat{q}$: solid line, the effective temperature from the present model, Eq. (34); dashed line, the effective temperature from EIT [5,6].

Introducing the drift velocity of the heat carriers V as $V = q/c_p T$, Eq. (34) can be rewritten as

$$\frac{\theta}{T} = \left(1 - \frac{V^2}{v^2}\right)^{1/2}. \tag{35}$$

Note that V characterizes collective motion of the heat carriers under nonequilibrium conditions, which leads to the nonzero heat flux. Taking into account that $v = h/\tau$ and $D = h^2/2\tau$, Eq. (35) can be presented in terms of the Peclet number $\mathrm{Pe} = Vh/D$ as

$$\frac{\theta}{T} = \left(1 - \frac{1}{4}\mathrm{Pe}^2\right)^{1/2}. \tag{36}$$

Note that the factor $\varphi = (1 - V^2/v^2)^{1/2}$ in Eq. (35) appears also as a scaling factor in the effective (thermal) diffusion length $h_{\mathrm{eff}} = \varphi h$ ahead of a fast moving heat source [12] or a phase transformation zone [19,25] due to using the HHCE in a moving reference frame $x \to x' - Vt$ [12,19,25]. The factor φ also arises in the different relativistic transformation laws of temperature [5], where the reference velocity v is the speed of light, whereas in the present model v is of the order of the speed of sound.

The effective heat capacity under the far-from-equilibrium condition is defined as $c_{\mathrm{neq}} = (\partial e/\partial\theta)_q$ [5,6,27]. The reason for this is that, according to the EIT [5,6], in a nonequilibrium steady state it is θ rather than T that is directly measured by a thermometer. Using Eq. (34), we obtain

$$c_{\mathrm{neq}}/c = (1 - \hat{q}^2)^{1/2}. \tag{37}$$

Equation (37) can be rewritten as $c_{\mathrm{neq}}/c = \theta/T$. When $|\hat{q}| \to 1$, Eqs. (34) and (37) give $\theta \to 0$ and $c_{\mathrm{neq}} \to 0$, respectively.

1. Low heat flux limit $|\hat{q}| \ll 1$

For relatively low heat flux $|\hat{q}| \ll 1$, one can expand Eqs. (34)–(37) in Taylor series, which gives

$$\frac{\theta}{T} = 1 - \frac{1}{2}\hat{q}^2, \tag{38}$$

$$\frac{\theta}{T} = 1 - \frac{1}{2}\frac{V^2}{v^2}, \tag{39}$$

$$\frac{\theta}{T} = 1 - \frac{1}{8}\mathrm{Pe}^2, \tag{40}$$

$$\frac{c_{\mathrm{neq}}}{c} = 1 - \frac{1}{2}\hat{q}^2. \tag{41}$$

Note that the low heat flux limit $|\hat{q}| \propto |q|/T \ll 1$, which can be reached either at low q or at high T, corresponds to the classical case [6,27]. According to a maximum entropy formalism of Camacho [27], the classical limit condition for the far-from-equilibrium state becomes a mere generalization of the equilibrium condition where the generalized temperature substitutes the equilibrium temperature, i.e., $\theta \gg T_D$, where T_D is the Debye temperature.

a. Interpretation of the effective temperature θ. Under the nonequilibrium conditions when $|\hat{q}| > 0$, a part of the kinetic energy used to compute the temperature T is not thermalized. It implies that Eq. (3) for the kinetic temperature T in one dimension can be presented as [39]

$$\frac{1}{2}k_B T = \left\langle \frac{m(w_i + V)^2}{2} \right\rangle \tag{42}$$

where $v_i = V + w_i$, with V being the local mean (drift) velocity, and w_i being the thermal randomized velocity of particle i, which corresponds to the thermalized kinetic energy. After some algebra Eq. (42) reduces to

$$\frac{1}{2}k_B T = \left\langle \frac{m w_i^2}{2} \right\rangle + \frac{1}{2}mV^2. \tag{43}$$

Taking into account that $\hat{q} = V/v$, Eq. (43) can be represented as

$$\left\langle \tfrac{1}{2}m w_i^2 \right\rangle \big/ \left(\tfrac{1}{2}k_B T\right) = 1 - \tfrac{1}{2}\alpha\hat{q}^2 \tag{44}$$

where $\alpha = 2v^2 m/Tk_B$. Comparison of Eq. (44) with Eq. (38) allows us to treat the effective temperature θ as the thermal temperature, which characterizes the thermalized (disordered) fraction of the local energy density, namely, $\frac{1}{2}k_B\theta = \langle \frac{1}{2}m w_i^2 \rangle$ (see also discussion in Refs. [5,6]). The energy of the "ordered" motion of the heat carriers is represented by the difference between the total energy density $\frac{1}{2}k_B T$ and the thermal fraction $\frac{1}{2}k_B\theta$, i.e., is given as $\frac{1}{2}k_B(T - \theta) \propto q^2 > 0$. During equilibration the energy of the ordered motion converts into the thermal energy of the disordered motion and, consequently, $\theta \to T$ at $q \to 0$ (see Fig. 1). Note that although θ is proportional to the thermal (equilibrated) fraction of the local energy density, it characterizes the nonequilibrium state and serves as a measure of how far from equilibrium the system is.

b. Comparison with gas hydrodynamics. Bernoulli's equation describing the adiabatic flow of ideal gas is given by [4]

$$\frac{T_V}{T_0} = 1 - \frac{(\gamma - 1)}{2}\frac{V^2}{v_0^2} \tag{45}$$

where T_V is temperature of the flowing gas, V is gas velocity, T_0 is gas temperature at $V = 0$, and v_0 is sound velocity at T_0. Equation (45) is similar to Eq. (39) if one identifies T_V, T_0, V, and v_0 in Ref. [4] with θ, T, V, and v in the present model. The analogy between Eqs. (45) and (39) is a manifestation of the energy conservation law for adiabatic systems, which allows the energy to transform from the kinetic form of the ordered motion into the thermal energy of the disordered motion. However, it should be noted that the analogy is not so straightforward because T in the present model characterizes both disordered (thermal) and ordered local energy, whereas T_0 in gas hydrodynamics is the classical thermodynamic temperature.

c. Comparison with the EIT. The EIT [5,6] goes beyond the local equilibrium assumption and obtains generalized heat conduction theory by introducing additional state variables, such as heat flux, into the expression of nonequilibrium entropy. As a result the nonequilibrium temperature θ_{EIT} is introduced by the EIT as follows [5,6]:

$$\frac{1}{\theta_{\mathrm{EIT}}} = \frac{1}{T} + \frac{\hat{q}^2}{2T}. \tag{46}$$

The EIT effective temperature θ_{EIT}, Eq. (46), is shown in Fig. 1 as a function of the nondimensional heat flux $\hat{q}$

(dashed line). Figure 1 clearly demonstrates that the effective temperatures from the present model θ, Eq. (34), and from the EIT $\theta_{\rm EIT}$, Eq. (47), agree well at a relatively small deviation from equilibrium when $|\hat{q}| \ll 1$, while at a high deviation from equilibrium when $|\hat{q}| \to 1$ the two temperatures differ substantially (compare solid and dashed curves in Fig. 1). The difference is due to the fact that $\theta_{\rm EIT}$ is obtained neglecting terms of order higher than q^2 [6]. Indeed, we can represent Eq. (38), which is an approximation of Eq. (34) with allowance for terms of order of q^2, as follows:

$$\frac{1}{\theta} = \frac{1}{T} + \frac{\hat{q}^2}{2\theta}. \tag{47}$$

Taking into account that for the small deviation from equilibrium $|\hat{q}| \ll 1$ the difference between the last terms on the right hand side of Eqs. (46) and (47) is small, these equations demonstrate very good agreement.

d. Comparison with the TMM. The TMM [41] indicates that the thermal energy is equivalent to a small amount of mass, called thermomass, according to Einstein's mass-energy equivalence relation. In dielectric bulk materials, the thermomass is represented by the phonon gas and the heat transport is thus regarded as the motion of phonon gas with a drift velocity. The momentum balance equation of phonon gas based on gas hydrodynamics [4] gives a generalized heat transport model, which agrees in many aspects with EIT [5,6]. Using Bernoulli's equation for phonon gas, Dong *et al.* [41] obtain the relation between the static temperature, $T_{\rm st}$ (effective temperature θ in the present model), and the total temperature, T_t (kinetic temperature in the present model), which corresponds to Eq. (39). For further comparison, we represent the equation for the static temperature $T_{\rm st}$ [Eq. (23) in Ref. [41]] as follows:

$$\frac{1}{T_{\rm st}} = \frac{1}{T_t} + \frac{\hat{q}^2}{T_{\rm st}^2/T_t}. \tag{48}$$

By comparison of Eqs. (46)–(48), it is inferred that at small deviation from equilibrium when the denominators in the last terms on the right hand side of these equations do not differ much, the results of the EIT, the TMM, and the present model agree quite well. However, for high deviation from equilibrium when $\hat{q} \to 1$, the results differ substantially (compare solid and dashed curves in Fig. 1).

e. Nonequilibrium temperature of active systems. The collective behavior of "active fluids," from swimming cells and bacteria colonies to flocks of birds or fishes, has raised considerable interest over the recent years in the context of nonequilibrium statistical physics [31,32,40]. The active systems consume energy from the environment or from internal fuel tanks and dissipate it by carrying out internal movements, which imply that their behavior is more ordered and thus intrinsically out of equilibrium. The energy input in active systems is located on internal units (e.g., motors) and therefore homogeneously distributed in the sample.

For the active systems, the definition of the effective temperature has come from the extensions of the FDT, that has been first introduced to study glasses [17]. The well-known Einstein relation $D = k_B T \mu$, where k_B is the Boltzmann constant, μ is the mobility, and D is the diffusion coefficient, expresses the relation between fluctuation (D) and response (μ). When manifested in a more general manner, this relation is called the fluctuation-dissipation theorem. The FDT states a general relationship between the response of a given system to an external disturbance and the internal fluctuations of the system in equilibrium. This relationship contains the temperature and is central in thermodynamics. However, when a system is out of equilibrium, the theorem breaks down and an extension of the theorem must be made. There is growing evidence that a modified form of the FDT with corresponding effective temperature holds out of equilibrium in a wide range of conditions, for example, in glassy systems in the ageing regime, jammed granular media, and nonequilibrium steady states in models of driven and active matter [32,40,47–49].

Palacci *et al.* [31] investigated experimentally the nonequilibrium steady state of an active colloidal suspension under gravity field. This paper yields a direct measurement of the effective temperature of the active system as a function of the particle activity, on the basis of the fluctuation-dissipation relationship. The effective temperature of the active colloids $T_{\rm eff}$ increases strongly with colloidal activity, which is characterized by the Peclet number $\mathrm{Pe}_S = r V_S / D_0$, where V_S is the swimming velocity, r is the colloid radius, and D_0 is the equilibrium diffusion coefficient, and is given by [32]

$$\frac{T_{\rm eff}}{T_0} = 1 + \frac{2}{9}\mathrm{Pe}_S^2 \tag{49}$$

where T_0 is a bath temperature. The active colloids consume energy from the environment in such a way that their motion begins to be more ordered, which increases the effective temperature $T_{\rm eff}$ in comparison with the bath temperature T_0. Compared with the present model, the bath (equilibrium) temperature T_0 corresponds to the effective thermal temperature θ, while $T_{\rm eff}$, which characterizes the more ordered motion of the active colloids in comparison with the equilibrium state, corresponds to the kinetic temperature T. To compare Eq. (49) with the present model, we rearranging Eq. (40) as follows:

$$\frac{T}{\theta} = 1 + \frac{1}{8}\mathrm{Pe}^2. \tag{50}$$

Taking into account that for active colloids Pe_S is defined in terms of the rotational time scale $\tau_r = 4r^2/3D$ [32], we infer that the result of the present model for small deviation from equilibrium, Eq. (50), agrees well with Eq. (49), obtained for the active systems on the basis of the fluctuation-dissipation theorem [32].

Ginot *et al.* [50] used sedimentation experiments to probe the nonequilibrium equation of state of a bidimensional assembly of active Janus microspheres and conduct computer simulations of a model of self-propelled hard disks. It has been shown that active colloids behave, in the dilute limit, as an ideal gas with an activity-dependent effective temperature, which also corresponds to Eqs. (49) and (50).

Multiple calculations of the effective temperature $T_{\rm eff}$ for self-propelled particles and motorized semiflexible filaments have been carried out with molecular dynamic simulations by Loi *et al.* [49] (see also review paper [40]). It has been demonstrated that the FDT allows for the definition of an effective temperature, which is compatible with the results obtained by using a tracer particle as a thermometer [40,47]. It was found that all data can be fitted by the empirical law

$T_{\rm eff}/T_b = 1 + \varepsilon f^2$, where f is the active force relative to the mean potential force, which plays a role analogous to the Peclet number for colloidal active particles used in the experiments [32], $\varepsilon = 15.41$ for filaments and $\varepsilon = 1.18$ for partials [47]. Thus, the empirical law obtained by Loi *et al.* [49] for the effective temperature in active systems is consistent with Eqs. (49) and (50).

2. *High heat flux limit* $|\hat{q}| \to 1$

When $|\hat{q}| \to 1$, Eqs. (34) and (37) give $\theta \to 0$ (see Fig. 1) and $c_{\rm neq} \to 0$, respectively. These results are consistent with the maximum entropy approach of Camacho [27], who has shown that the high heat flux limit $|\hat{q}| \to 1$ corresponds to the quantum case $\theta \ll T_D$. Thus, the present model provides reasonable results both in the classical ($|\hat{q}| \ll 1$) and in the quantum ($|\hat{q}| \to 1$) limits, whereas the EIT and the TMM are valid only for relatively small deviation from equilibrium $|\hat{q}| \ll 1$ in the classical limit $\theta \gg T_D$. Indeed, the TG representation, used in the present model [see Eqs. (30) and (31)], corresponds to the Debye approximation in the maximum entropy formalism [27] when one can split the nonequilibrium phonon distribution function in two Bose-Einstein distributions for phonons moving to the left and phonons moving to the right, respectively. As the heat flux increases, the temperature for the phonons moving along the heat flux, T_1, increases [see Eq. (30)], whereas the temperature for the phonons moving against the heat flow, T_2, decreases so as $T_2 \to 0$ at $|\hat{q}| \to 1$ [see Eq. (31)]. This indicates that the limit $|\hat{q}| \to 1$ cannot be addressed classically: in this limit, the number of phonons moving against the heat flux is too low so as to permit the classical limit to apply [27]. Thus, the present model due to the TG representation is consistent with the Bose-Einstein statistics and gives expressions for the effective temperature θ, Eq. (34), and corresponding nonequilibrium heat capacity $c_{\rm neq}$, Eq. (37), which cover both the quantum, $|\hat{q}| \to 1$ and $\theta \ll T_D$, and the classical, $|\hat{q}| \ll 1$ and $\theta \gg T_D$, limits.

For further consideration it is convenient to represent Eq. (33) in a slightly different form:

$$T^2 = \theta^2 + (q/cv)^2. \tag{51}$$

In the quantum limit for n-dimensional space the local energy density e is proportional to T^{1+n} [51], which for one dimension gives $e \propto T^2$ [6,27,51]. Thus, Eq. (51) is similar to the energy conservation law $e = e_{\rm therm} + e_{\rm ord}$, where $e \propto T^2$ is the local energy density, which is the sum of the thermal (disordered) fraction $e_{\rm therm} \propto \theta^2$ and the ordered fraction $e_{\rm ord} \propto q^2$. According to the Debye model $c \propto T^3$ in three dimensions at low temperatures [3]. For n-dimensional space $c \propto T^n$, which for one dimension gives $c \propto T$. When $\hat{q} \to 1$, Eq. (37) gives $c_{\rm neq} \propto \theta$, which implies a generalization of the Debye model for heat capacity in the low temperature quantum limit to the nonequilibrium situation. In n-dimensional space it is expected that $c_{\rm neq} \propto \theta^n$.

Disordered semiconductors. The non-linear relation for the effective temperature has been observed in disordered semiconductors under electric field [5,43–48]. When an electric field is applied to a semiconductor one can characterize the combined effects of the field and the lattice temperature by an effective temperature to describe carrier drift mobility, dark conductivity, and photoconductivity [5,43–46]. Marianer and Shklovskii [43] on the basis of their numerical calculations of the linear balance equation for electron transition between localized states in an exponential tail have obtained the heuristic formula for the effective temperature:

$$T_{\rm eff}^2 = T_0^2 + (Ae_{\rm el}El/k_B)^2 \tag{52}$$

where $T_{\rm eff}$ is the effective temperature of the crystal under electric field, T_0 is the crystal temperature with zero electric field, E is the electric field, l is the localization length and $e_{\rm el}$ is the electron charge, and $A \approx 0.67$. Baranovskii *et al.* [44] verified the concept of the effective temperature for the distribution of electrons in band tails under the influence of a high electric field using a new Monte-Carlo simulation algorithm. The simulated data demonstrated a good agreement with the phenomenological equation (52) in a wide temperature range $3 < T < 150$ K. These results indicate that the concept of the effective temperature can in fact be used as a substitute for the combined action of both the applied electric field and the temperature, as far as relaxation processes are concerned [44]. Nebel *et al.* [45], who experimentally measured the electric-field-dependent dc dark conductivity over a broad temperature range ($10 < T < 300$ K) in phosphorus- and boron-doped and intrinsic amorphous hydrogenated silicon (a-Si:H), found a good agreement with the phenomenological expression, Eq. (52). Liu and Soonpaa [46] experimentally demonstrated the similarity between temperature and electric-field effects in thin crystals of $Bi_{14}Te_{11}S_{10}$ and observed a good agreement with Eq. (52), particularly at low temperatures from $T = 1.8$ to 4.5 K. Liu and Soonpaa noted that the quantum effects played an important role in their experiments due to the sample size of five atoms thick and the low temperatures. Note that although the heuristic Eq. (52) provides a good comparison with the experimental data [44,45] and is helpful from a practical point of view, it did not obtain a physical interpretation [5,45].

Compared with the present model, the crystal temperature with zero electric field T_0 corresponds to the effective temperature θ, while the effective temperature of the crystal under electric field $T_{\rm eff}$ corresponds to the kinetic temperature T. Taking into account that the electric current $i = \sigma_E E$, where σ_E is the electrical conductivity, plays an analogous role as the heat flux q (see, for example, Ref. [6]), we obtain that the heuristic Eq. (52) corresponds to the prediction of the present model, Eq. (51).

More recently, Pachoud *et al.* [47] experimentally investigated electron transport in granular graphene films self-assembled by hydrogenation of suspended graphene. The authors measured the conductance G of different bias voltages U and temperatures T to extract the typical localization length of the samples l at different temperatures between 2.3 and 20 K. It was shown that charge carriers experience an effective temperature $T_{\rm eff}$, which is described by Eqs. (51) and (52). Importantly, $T_{\rm eff}$ uniquely determines G, which implies that constant-conductance domains of (U^2, T^2) space are straight lines of slope $(Ae_{\rm el}l/L_{\rm ch}k_B)^2$, where $L_{\rm ch}$ is the channel length and $L_{\rm ch} = U/E$ [47]. It has been also demonstrated that two different regimes can be clearly distinguished in the behavior of the standard deviations $\sigma_{\ln G}$ of the log conductance as a function of $T_{\rm eff}$: below $T_{\rm eff} = 10$ K, $\sigma_{\ln G}$ is weakly temperature dependent while, above 10 K, $\sigma_{\ln G}$ decreases rapidly with $T_{\rm eff}$.

This implies that the concept of the effective temperature is very useful for analyzing transport phenomena in the granular graphene materials [47].

Abdalla *et al.* [48] investigated the scalability of the temperature and electric-field dependence of the conductivity of disordered organic semiconductors by using the effective temperature concept. It has been demonstrated that the scaling phenomena can have their physical origin in a simple heat balance of Joule heating and energy-dependent relaxation [48], which corresponds to the physical origin of the effective temperature in the present model (see discussion in Secs. III A 1 a and III A 2). However, depending on the used input parameters, both the numerical and the empirical model developed by Abdalla *et al.* [48] show smaller or larger deviations from the ideal scaling behavior, Eq. (52). The discrepancy may be caused by the difference between the electron and lattice temperatures under nonequilibrium conditions, which is usually described on the basis of the two temperature (TT) approach [12,13,34,53–55]. Generalization of the present model to the TT approach for semiconductors [53–55] is not a trivial matter; however, the similarity between the effective temperature θ, Eq. (51), and the scaling behavior of the temperature- and electric-field dependence of the conductivity of semiconductors [43–48] seems to be intriguing and is an important topic for future work.

Thus, Eq. (33) for the effective temperature θ corresponds to the results of the EIT [5,6], the TMM [41], and the FDT approach for active systems [32,40,47–49] at small deviation from equilibrium, whereas at high deviation from equilibrium it agrees with the maximum entropy formalism of Camacho [27] in the quantum limit and the empirical relation for the effective temperature of disordered semiconductors under electric field [5,43–48]. This implies that the definition of the effective temperature, Eq. (33), can be used for systems of different physical nature in a wide range of deviation from equilibrium.

3. Some comments

a. Space-time evolution of the effective temperature. It should be stressed that the space-time evolution of the kinetic temperature T is governed by the HHCE with corresponding (nonequilibrium) boundary conditions. The space-time evolution of the heat flux is governed by the MFL, which contains the gradient of T, not of θ. However, the space-time evolution of the effective temperature θ can be calculated in two ways. The first way is to calculate T and q using the HHCE and the MFL, which gives θ using Eq. (33). Another way is to calculate T_1 and T_2 using the HHCE and then calculate θ from Eq. (32). Note that although the space-time evolutions of T, T_1, and T_2 are governed by the same HHCE, Eq. (2), they do not coincide due to different boundary and initial conditions.

b. Effective and reference temperatures. An effective temperature is usually introduced as an additional variable which serves as a measure of how far from equilibrium the system is, while corresponding equilibrium temperature is considered as a reference temperature. The effective temperature of active systems $T_{\rm eff}$ characterizes the nonequilibrium state and depends on the consumed energy from the environment, while the ambient (equilibrium) bath temperature T_0 plays a role of the reference temperature [32,40,47,49]. Analogously in the disordered semiconductors [43–46,48], $T_{\rm eff}$ characterizes the nonequilibrium state under external electric field, while the equilibrium crystal temperature at zero electric field T_0 plays the role of the reference temperature. In these cases $T_{\rm eff} \geqslant T_0$.

The effective temperature of the passive relaxing systems θ describes how far from equilibrium the system is and, in this sense, θ is similar to $T_{\rm eff}$. However, θ characterizes the thermal (equilibrated) fraction of the local energy density and, in this sense, disagrees with $T_{\rm eff}$, but corresponds to the equilibrium bath temperature T_0. The kinetic temperature of the passive relaxing systems T characterizes the local energy density of the nonequilibrium state and, in this sense, is similar to $T_{\rm eff}$. However, during relaxation to equilibrium (see Sec. IV A), the thermal effective temperature θ increases due to thermalization process, whereas T is kept constant and plays the role of the reference temperature. Thus, there are some similarities and differences between the effective and reference temperatures of the active and passive relaxing systems with heat flux. Therefore, it is important not to be confused concerning the definitions of effective and reference temperatures under far-from-equilibrium conditions (see also discussion in Ref. [5]).

B. Effective entropy

The information entropy is given by [3]

$$S_{\rm neq} = -\sum_i u_i \ln u_i$$

where u_i is the distribution function of subsystem i. For the system under consideration we have two subsystems ($i = 1,2$), the distribution function of which can be represented in terms of the corresponding temperatures as $u_i = T_i/2T$. In such a case this equation takes the form

$$S_{\rm neq} = -[T_1 \ln(T_1/2T) + T_2 \ln(T_2/2T)]/2T.$$

Using Eqs. (30) and (31) for T_i, the expression for entropy under far-from-equilibrium conditions can be rewritten in terms of heat flux as

$$S_{\rm neq} = \ln 2 - \tfrac{1}{2}(1+\hat{q})\ln(1+\hat{q}) - \tfrac{1}{2}(1-\hat{q})\ln(1-\hat{q}). \tag{53}$$

The nonequilibrium entropy $S_{\rm neq}$, Eq. (53), scaled with $S_{\rm eq}$, is shown in Fig. 2 as a function of the nondimensional heat flux $\hat{q}$ (solid line). As expected, S is always less than or equal to that of a local equilibrium situation $S_{\rm eq} = \ln 2$. The presence of the heat flux reduces the value of $S_{\rm neq}$, indicating that the nonequilibrium state is more ordered than the corresponding equilibrium state.

The Lagrange multiplier γ assigned to the heat flux constraint can be calculated as

$$\gamma = \left(\frac{\partial S_{\rm neq}}{\partial q}\right)_e = -\frac{1}{2}\ln\frac{1+\hat{q}}{1-\hat{q}}. \tag{54}$$

The parameter γ has no analog in equilibrium and must be regarded as a purely nonequilibrium quantity describing how an increment in the heat flux modifies the entropy [6,27]. Figure 3 shows minus γ calculated from Eq. (54) as a function of $\hat{q}$.

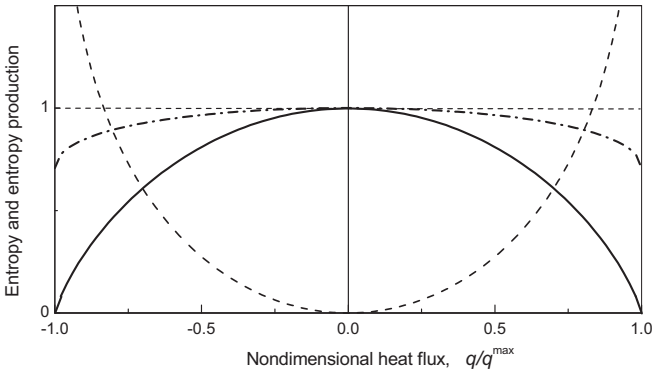

FIG. 2. Nonequilibrium entropy S_{neq}, Eq. (45), scaled with S_{eq} (solid line) and the entropy production σ_S, Eq. (46) (dashed line), as functions of the nondimensional heat flux $\hat{q}$. The nonequilibrium entropy obtained by Camacho [27] from a maximum entropy formalism is placed for comparison (dash-dotted line).

To introduce the corresponding entropy production σ_S, let us consider, following the EIT [5,6], a volume element which is sufficiently small so that within it the spatial variation of temperature is negligible. If the volume element is suddenly isolated and allowed to decay to equilibrium, the entropy production would be $\sigma_S = \dot{S}_{neq} = \gamma \partial\hat{q}/\partial t'$, where $t' = t/\tau$ is the nondimensional time. Taking into account that for the small volume element Eq. (1) gives $\partial\hat{q}/\partial t' = -\hat{q}$, the entropy production can be expressed as

$$\sigma_S = -\frac{\hat{q}}{2} \ln \frac{1+\hat{q}}{1-\hat{q}}. \tag{55}$$

Figure 2 shows σ_S as a function of $\hat{q}$ (dashed line). In equilibrium $\hat{q} = 0$ and, as expected, $\sigma_S = 0$. When $\hat{q} \to 1$, Eq. (55) gives $\sigma_S \to \infty$.

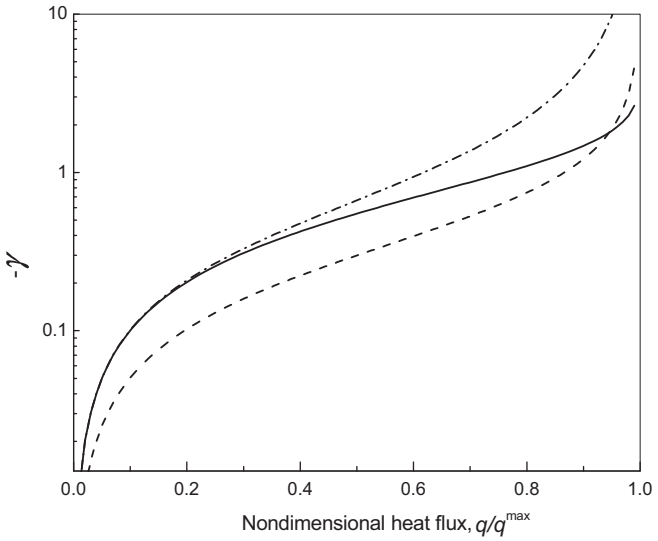

FIG. 3. Parameter minus γ as a function of the nondimensional heat flux $\hat{q}$: solid line, the present model; dashed line, the quantum limit by Camacho [27]; dash-dotted line, the classical limit by Camacho [27].

Note that the 1D approach for heat transfer under far-from-equilibrium conditions has proved to be very useful in many applications [1,2,5,6,11,15–17,27,28,37,38,42], particularly for low dimensional nanosystems [11,15–17,37,38,42]. Moreover, following a maximum entropy formalism, Camacho [27] demonstrated that 1D and three-dimensional (3D) models for crystals under heat flux give the same asymptotic behavior of the effective temperature and the nonequilibrium Lagrange multiplier γ in the quantum limit [27]. Generalization of the present 1D model to the two-dimensional and 3D case can be based on the LBM [36,37,42], the DVM [34], and cellular automata [52] approaches; however, it is not a trivial matter and it will be an important topic of future work.

1. Low heat flux limit $|\hat{q}| \ll 1$

For a relatively low heat flux $\hat{q} \ll 1$, the expression for the entropy S, Eq. (53), and the entropy production σ_S, Eq. (55), can be expressed as

$$S_{neq} = S_{eq} - \hat{q}^2/2, \tag{56}$$

$$\sigma_S = \hat{q}^2, \tag{57}$$

which agree with the expression for the local nonequilibrium entropy and the entropy production obtained by Jou and coworkers [5,6] in the framework of the EIT and by Dong *et al.* [41] in the framework of the TMM. In the limit the parameter γ reduces to $\gamma = -\hat{q}$, which corresponds to the classical limit by Camacho [27] (compare solid and dash-dotted lines in Fig. 3). Moreover, Eq. (56) corresponds to the dependence of the entropy on the order parameter in the Landau theory of second-order phase transition [3]. This indicates that $\hat{q}$ plays a role similar to that of the order parameter. Indeed, the nondimensional heat flux $\hat{q}$ varies from $\hat{q} = 0$ in the equilibrium (completely disordered) state to $\hat{q} = 1$ in the completely ordered state, when all the particles move in the same direction. As we discussed above, the low heat flux $\hat{q} \propto q/T_k \ll 1$ corresponds to the classical high temperature limit.

2. High heat flux limit $|\hat{q}| \to 1$

When $|\hat{q}| \to 1$, i.e., in the quantum limit, Eq. (53) for the nonequilibrium entropy S_{neq} results in $S_{neq} \to 0$ (see solid line in Fig. 2), whereas Eq. (55) for the entropy production σ_S gives $\sigma_S \to \infty$ (see dashed line in Fig. 2). This can be understood microscopically as follows: as the heat flux grows, the number of heat carriers moving contrary to the heat flow decreases, and in the limit $|\hat{q}| \to 1$ they disappear. This implies that the nonequilibrium state begins to be more ordered and corresponding entropy, Eq. (53), tends to zero.

Thus, the present model provides a generalization of the third law to nonequilibrium states: indeed, when $|\hat{q}| \to 1$, Eqs. (53), (34), and (37) predict that $S_{neq} \to 0$, $\theta \to 0$, and $c_{neq} \to 0$, respectively, even at a nonzero value of T (see also discussion about the third law in Refs. [5,6,27]).

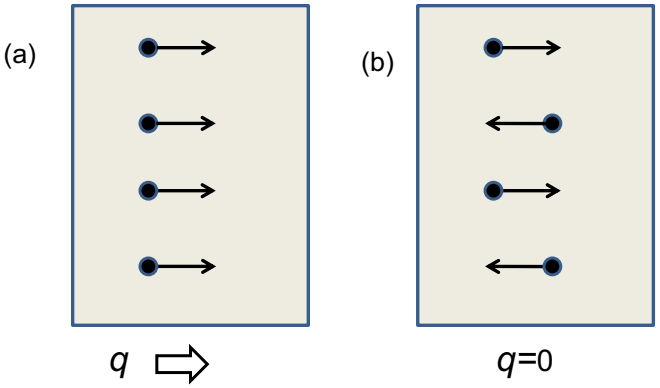

FIG. 4. (a) Schematic representation of the nonequilibrium state with the maximum heat flux $q = q^{\max}$ when all the heat carriers move in the same direction. In this case $T_1 = 2T$, $T_2 = 0$, and $\theta = 0$. (b) Schematic representation of the equilibrium state with $q = 0$. In this case $T_1 = T_2 = \theta = T$.

IV. ILLUSTRATIVE EXAMPLES

A. Effective temperature in monatomic ideal gas

Let us consider a virtual relaxation to local equilibrium of a small adiabatically isolated system where the heat carriers are placed uniformly and move in the same direction. In other words, the initial condition for the situation is $q = q^{\max}$ at the initial time moment $t = 0$ [see Fig. 4(a)]. In this case Eqs. (30) and (31) give the initial conditions for the temperatures T_1 and T_2 as follows: $T_1 = 2T$ and $T_2 = 0$, while Eq. (32) gives $\theta = 0$. As we discussed above, the heat flux in the system is governed by the equation $\partial\hat{q}/\partial t' = -\hat{q}$, which gives $\hat{q}(t) = \exp(-t/\tau)$ (see also [5,6]). Accordingly, the temperatures, T_1 and T_2, tend to the equilibrium temperature T as $T_1 = T[1 + \exp(-t/\tau)]$ and $T_2 = T[1 - \exp(-t/\tau)]$, respectively (see dashed lines in Fig. 5). The effective temperature θ increases from zero at $t = 0$ to its maximum value $\theta^{\max} = T$ in the equilibrium state at $t \to \infty$ (see solid line in Fig. 5). Figure 6 shows the time evolution of the nonequilibrium entropy $S_{\rm neq}$, Eq. (53), scaled with S_{eq} (solid line) and corresponding entropy production σ_S, Eq. (55) (dashed line). As expected, $S_{\rm neq}/S_{\rm eq}$ increases from zero at $t = 0$ to unity at equilibrium at $t \to \infty$ (solid line in Fig. 6), whereas σ_S decreases from at $t = 0$ to zero in equilibrium at $t \to \infty$ (dashed line in Fig. 6)

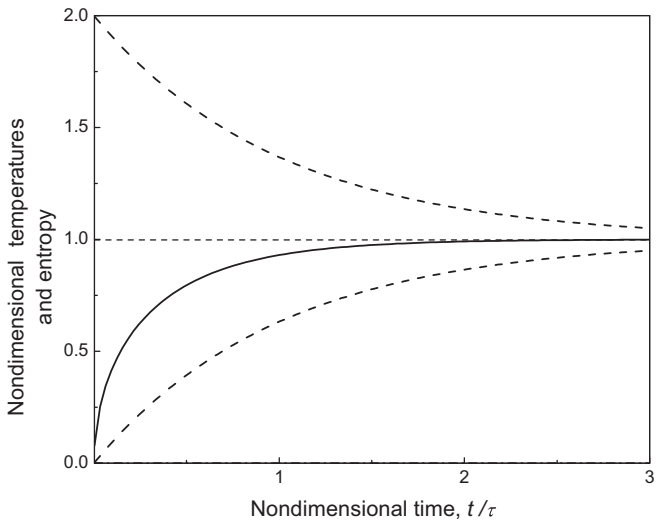

FIG. 5. Nondimensional effective temperature θ/T (solid line) as a function of nondimensional time t/τ during relaxation from the nonequilibrium state [see Fig. 4(a)] to the equilibrium state [see Fig. 4(b)]. The temperatures T_1/T (upper dashed line) and T_2/T (bottom dashed line) are also shown for comparison.

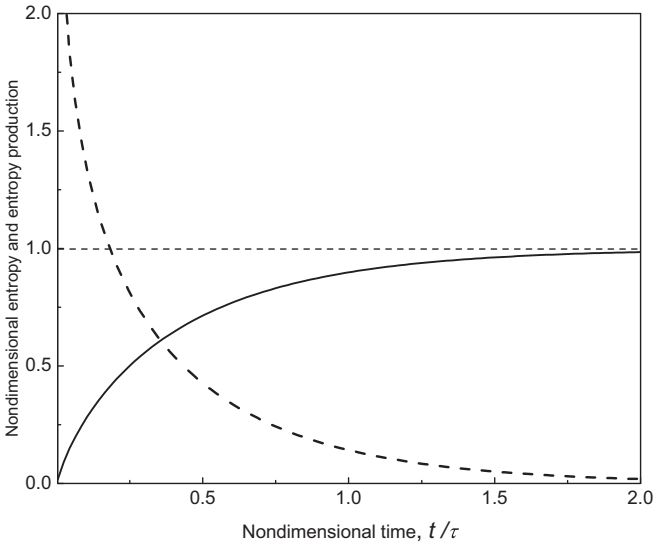

FIG. 6. Nonequilibrium entropy $S_{\rm neq}$, Eq. (45), scaled with $S_{\rm eq}$ (solid line) and the entropy production σ_S, Eq. (46) (dashed line), as functions of nondimensional time t/τ during relaxation from the nonequilibrium state [see Fig. 4(a)] to the equilibrium state [see Fig. 4(b)].

The time evolution of T_1 and T_2 is analogous to the behavior of the effective temperatures for a birth-death process in gene networks [32]: as the coupling strength between species increases, the effective temperatures of the species tend to equalize, as the "hotter" one drops and the "cooler" one increases, reaching the average temperature [compare Fig. 5 in the present paper with Fig. 4(a) in Ref. [32]].

Now let us compare the behavior of T_1, T_2, and θ in the present model (Fig. 5) with the LBM simulation of pico- and femtosecond laser heating of silicon [42]. In spite of the fact that the LBM simulation calculates the temperature distribution in the bulk silicon as a function of coordinate, whereas the present model gives the temperatures as a function of time, the results can be qualitatively compared because they both consider the energy evolution due to interaction (relaxation) between different modes. So, after the laser heating in LBM simulation [42] stops, the equivalent temperature in the laser incidence direction, which corresponds to T_2 in the present paper, decreases with coordinate, while the equivalent temperature in the opposite direction, which corresponds to T_1 in the present model, increases. This behavior exactly corresponds to the time evolution of T_2 and T_1 (see Fig. 5). Moreover, the equivalent temperature in the LBM simulation [42], associated with the energy flowing in one of the lateral directions, increases with coordinate in analogy to the increase of the effective temperature θ in time (see solid curve in Fig. 5). Both temper-

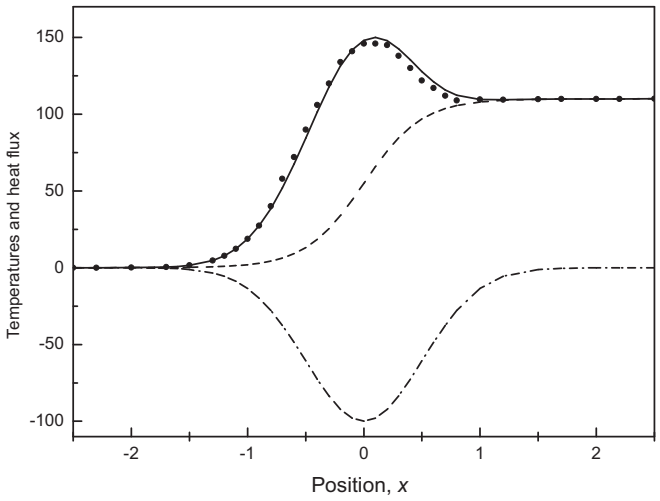

FIG. 7. Nondimensional temperatures and heat flux distributions as functions of coordinate x for a strong shockwave ($x = 0$ is the wave front). The solid line denotes the longitudinal component of the temperature in the direction of the shockwave T (or T_{xx} in terms of Ref. [30]) calculated from Eq. (34); solid circles denote the nonequilibrium molecular dynamics simulation data for T_{xx} [30]; the dashed line and dash-dotted line denote the average (or effective) temperature θ and the heat flux q, respectively, taken from Ref. [30].

atures increase due to equalization of the initially nonuniform distribution of energy between different degrees of freedom.

B. Effective temperature in shock wave: Comparison with MD simulation

The shock-wave propagation occurs under strong nonequilibrium conditions because the shock front is highly localized in both distance (a few interatomic spacings) and time (a few mean collision times) [30]. Due to the far-from-equilibrium nature of the shock wave the average kinetic temperature T_k is defined in terms of the local peculiar kinetic energy; hence T is one-third the trace of the kinetic temperature tensor [30]. In the shock front, the kinetic temperature component in the direction of shock propagation, T_{xx}, is higher than the transverse components, T_{yy} and T_{zz}, which are equal to each other by symmetry. Therefore T_k is also always lower than T_{xx}, except at equilibrium, which occurs long before the shock has arrived and long afterwards, when equipartition holds. Moreover, T_{xx} shows a distinct peak near the center of the shock front, and this disequilibrium is due to collisions in the shock compression process [30]. The temperatures T_{xx} and T_k in the work of Holian *et al.* [30] correspond to T and θ in the present model, respectively. To compare the MD results with the present model, we take the data for $q(x)$ and $\theta(x)$ from Fig. 3 in Ref. [30] and then calculate T (analog to T_{xx}) from Eq. (34). All the functions were normalized to the corresponding equilibrium values at $x \to \infty$ taken from [30], so we do not need to know the heat capacity and phonon speed to calculate T from Eq. (34). Figure 7 shows the effective (average) temperature θ (dashed curve), the longitudinal component of temperature in the shock-wave direction T from Eq. (34) (solid curve), the MD data for T_{xx} from Ref. [30] (solid circles), and the heat flux q (dash-dotted curve) as a function of coordinate x for a strong shockwave in the Lennard-Jones dense fluid ($x = 0$ is the wave front). Comparison of the behavior of T calculated from the present model (solid curve in Fig. 7) and the nonequilibrium MD data for T_{xx} (solid circles) taken from Ref. [30] demonstrates good agreement. Thus, the present model, Eq. (34), correctly describes the relationship between the temperatures, T_{xx} and T_k, and the heat flux q in the front of the strong shock waves. Note that a distinct peak of the longitudinal temperature near the wave front due to nonequilibrium effects has been predicted earlier around a fast-moving heat source [12].

V. CONCLUSION

The random walk with a finite value of the heat (mass) carrier velocity [1,2], as well as the DVM with the wave law of the continuum limit [12,13,26,34–36] and the BTE with the single relaxation time approximation [6,10,18,24,37,38,42], lead to the HHCE, Eq. (2), and the MFL, Eq. (1). The HHCE describes the space-time evolution of the kinetic temperature T, which characterizes the local energy density under far-from-equilibrium conditions. The thermalized (disordered) fraction of the local energy density is characterized by the effective temperature θ, which is a nonlinear function of T and heat flux q, Eq. (34). In equilibrium $q = 0$ and $\theta = T$, whereas out of equilibrium $|q| > 0$ and $\theta < T$. In the quantum limit $q \to q_{\max}$, where $q_{\max}$ is the maximum possible value of the heat flux reached when all the heat carriers move in the same directions, $\theta \to 0$, $c_{\rm neq} \to 0$, and $S_{\rm neq} \to 0$ even at $T > 0$. This provides a generalization of the third law to the nonequilibrium situation.

Thus the present model captures well the behavior of the effective temperature and entropy in systems with heat flux both in the classical and in the quantum limits. The definition of the effective temperature can be also used for nonpassive systems, such as active biosystems and systems under external fields. However, a comprehensive formulation of the concepts of nonequilibrium temperature and entropy for more complex systems, particularly in the quantum limit, is still an open problem and requires additional research.

ACKNOWLEDGMENT

The reported study was supported by the Russian Foundation for Basic Research, Research Project No. 16-03-00011.

[1] V. A. Fock, Trans. Opt. Ins. Leningrad **4**, 1 (1926).
[2] B. I. Davydov, Dokl. Akad. Nauk SSSR **2**, 474 (1935) [C. R. Acad. Sci. URSS **2**, 476 (1935)].
[3] L. D. Landau and E. M. Lifshitz, *Statistical Physics* (Pergamon, Oxford, 1970).
[4] L. D. Landau and E. M. Lifshitz, *Fluid Mechanics* (Pergamon, Oxford, 1966).
[5] J. Casas-Vázquez and D. Jou, Rep. Prog. Phys. **66**, 1937 (2003).
[6] D. Jou, J. Casas-Vázquez, and G. Lebon, *Extended Irreversible Thermodynamics* (Springer, Berlin, 2010).

[7] P. Ván and T. Fülöp, Ann. Phys. (Berlin) **524**, 470 (2012).
[8] R. E. Nettleton and S. L. Sobolev, J. Non-Equilibr. Thermodyn. **20**, 205 (1995); **20**, 297 (1995); **21**, 1 (1996).
[9] S. L. Sobolev, Phys. Lett. A **381**, 2893 (2017).
[10] Y. Guo and M. Wang, Phys. Rep. **595**, 1 (2015).
[11] S. Lepri, R. Livi, and A. Politi, Phys. Rep. **377**, 1 (2003).
[12] S. L. Sobolev, Usp. Fiz. Nauk. **161**, 5 (1991) [Sov. Phys. Usp. **34**, 217 (1991)].
[13] S. L. Sobolev, Usp. Fiz. Nauk. **167**, 1095 (1997) [Phys.–Usp. **40**, 1043 (1997)].
[14] D. D. Joseph and L. Preziosi, Rev. Mod. Phys. **61**, 41 (1989); **62**, 375 (1990).
[15] H. G. Weiss, Physica A **311**, 381 (2002).
[16] D. G. Cahill, W. K. Ford, K. E. Goodson, G. D. Mahan, A. Majumdar, H. J. Maris, R. Merlin, and S. R. Phillpot, J. Appl. Phys. **93**, 793 (2003).
[17] Y. Dubi and M. Di Ventra, Rev. Mod. Phys. **83**, 131 (2011); J. Kurchan, Nature (London) **433**, 222 (2005).
[18] S. Sinha and K. E. Goodson, Int. J. Multiscale Comput. Eng. **3**, 107 (2005).
[19] S. L. Sobolev, Mater. Sci. Technol. **31**, 1607 (2015).
[20] M. E. Siemens, Q. Li, R. Yang, K. A. Nelson, E. H. Anderson, M. M. Murnane, and H. C. Kapteyn, Nat. Mater. **9**, 26 (2010).
[21] M. Criado-Sanchoa, D. Jou, and J. Casas-Vázquez, Phys. Lett. A **350**, 339 (2006).
[22] G. Chen, J. Heat Transf. **118**, 539 (1996); **124**, 328 (2002).
[23] W. Liu, K. Saanouni, S. Forest, and P. Hu, J. Non-Equilibr. Thermodyn. **42**, 327 (2017)
[24] A. Majumdar, J. Heat Transf. **115**, 7 (1993).
[25] S. L. Sobolev, Phys. Rev. E **55**, 6845 (1997).
[26] S. L. Sobolev, Int. J. Heat Mass Transf. **108**, 933 (2017).
[27] J. Camacho, Phys. Rev. E **51**, 220 (1995).
[28] E. Kronberg, A. H. Benneker, and K. R. Westerterp, Int. J. Heat Mass Transf. **41**, 127 (1998).
[29] P. K. Patra and R. C. Batra, Phys. Rev. E **95**, 013302 (2017).
[30] B. L. Holian, M. Mareschal, and R. Ravelo, Phys. Rev. E **83**, 026703 (2011).
[31] J. Palacci, C. Cottin-Bizonne, C. Ybert, and L. Bocquet, Phys. Rev. Lett. **105**, 088304 (2010).
[32] T. Lu, J. Hasty, and P. G. Wolynes, Biophys. J. **91**, 84 (2006).
[33] C. Essex, R. McKitrick, and B. Andresen, J. Non-Equilibr. Thermodyn. **32**, 1 (2007).
[34] S. L. Sobolev, J. Phys. III France **3**, 2261 (1993).
[35] S. L. Sobolev, Int. J. Heat Mass Transf. **71**, 295 (2014).
[36] A. Nabovati, D. P. Sellan, and C. H. Amon, J. Comput. Phys. **230**, 5864 (2011).
[37] R. A. Escobar, S. S. Ghai, M. S. Jhon, and C. H. Amon, Int. J. Heat Mass Transf. **49**, 97 (2006).
[38] S. Pisipati, J. Geer, B. Sammakia, and B. T. Murray, Int. J. Heat Mass Transf. **54**, 3406 (2011).
[39] S. Volz, J.-B. Saulnier, M. Lallemand, B. Perrin, P. Depondt, and M. Mareschal, Phys. Rev. B **54**, 340 (1996).
[40] C. Bechinger, R. Di Leonardo, H. Löwen, C. Reichhardt, G. Volpe, and G. Volpe, Rev. Mod. Phys. **88**, 045006 (2016); L. F. Cugliandolo, J. Phys. A: Math. Theor. **44**, 483001 (2011).
[41] Y. Dong, B. Y. Cao, and Z. Y. Guo, Phys. Rev. E **87**, 032150 (2013).
[42] J. Xu and X. Wang, Physica B **351**, 213 (2004).
[43] S. Marianer and B. I. Shklovskii, Phys. Rev. B **46**, 13100 (1992).
[44] S. D. Baranovskii, B. Cleve, R. Hess, and P. Thomas, J. Non-Cryst. Solids **164-166**, 437 (1993).
[45] C. E. Nebel, R. A. Street, N. M. Johnson, and C. C. Tsai, Phys. Rev. B **46**, 6803 (1992).
[46] G. Liu and H. H. Soonpaa, Phys. Rev. B **48**, 5682 (1993).
[47] A. Pachoud, M. Jaiswal, Yu. Wang, B.-H. Hong, J.-H. Ahn, K. P. Loh, and B. Ozyilmaz, Sci. Rep. **3**, 3404 (2013).
[48] H. Abdalla, K. Van de Ruit, and M. Kemerink, Sci. Rep. **5**, 16870 (2015).
[49] D. Loi, S. Mossa, and L. F. Cugliandolo, Soft Matter **7**, 3726 (2011); **7**, 10193 (2011).
[50] F. Ginot, I. Theurkauff, D. Levis, C. Ybert, L. Bocquet, L. Berthier, and C. Cottin-Bizonne, Phys. Rev. X **5**, 011004 (2015).
[51] P. T. Landsberg and A. De Vos, J. Phys. A **22**, 1073 (1989).
[52] Y. Zhao, R. Qin, D. Chen, X. Wan, Y. Li, and M. Ma, Steel Research Int. **86**, 1490 (2015).
[53] A. F. Carballo Sánchez, G. González de la Cruz, Yu G. Gurevich, and G. N. Logvinov, Phys. Rev. B **59**, 10630 (1999).
[54] G. G. de la Cruz and Yu. G. Gurevich, Semicond. Sci. Technol. **26**, 025011 (2011).
[55] Yu. G. Gurevich and A. Ortiz, J. Phys. D **41**, 065410 (2008).